

How do chiral condensates affect color superconducting quark matter under charge neutrality constraints?

Hiroaki Abuki,^{1,*} Masakiyo Kitazawa,^{1,2,†} and Teiji Kunihiro^{1,‡}

¹*Yukawa Institute for Theoretical Physics, Kyoto University, Kyoto 606-8502, Japan*

²*Department of Physics, Kyoto University, Kyoto 606-8502, Japan*

(Dated: November 9, 2018)

We investigate the effects of the dynamical formation of the chiral condensates on color superconducting phases under the electric and color neutrality constraints at vanishing temperature. We shall show that the phase appearing next to the color-flavor-locked (CFL) phase down in density depends on the strength of the diquark coupling. In particular, the gapless CFL (gCFL) phase is realized only in a weak coupling regime. We give a qualitative argument on why the gCFL phase in the weak coupling region is replaced by some other phases in the strong coupling, once the competition between dynamical chiral symmetry breaking and the Cooper pair formation is taken into account.

PACS numbers: 12.38.-t, 25.75.Nq

On the basis of the asymptotic-free nature of QCD and the attraction between quarks due to gluon exchanges, we now believe that the ground state of the quark matter composed of u, d and s quarks at extremely high densities is a special type of color superconducting phases [1, 2]; that is the color-flavor locked (CFL) phase where all the quarks equally participate in pairing [3, 4].

In reality, nature may not, however, allow such an extremely high-density matter to exist, even in the core of neutron stars and in possible quark stars. In such systems at relatively low density corresponding to the quark chemical potential of, say, 500 MeV, the following two ingredients become important for the fate of the CFL phase and determining the pattern of color superconductivities [5, 6, 7]: Firstly, one can not neglect the effect of the strange quark mass M_s , which ranges from around 100 MeV to 500 MeV depending on the quark density. Secondly, the constraints of the color and electric neutrality must be satisfied as well as β -equilibrium under the weak interaction. The former causes Fermi-momentum mismatch [8, 9, 10], and the latter pulls up or down the Fermi momentum of each species of quarks [6, 7]; as the density goes lower, the symmetric CFL pairing would cease to be the ground state at some critical density, and some phases other than the CFL phase would appear.

One of the recent findings of such novel pairing patterns is the gapless CFL (gCFL) phase [11, 12], which is a non-BCS state having some quarks with gapless dispersions despite the same symmetry breaking pattern as the CFL phase. Historically, a possible realization of the stable gapless state was first discussed for the two-flavor color superconducting phase [13]: It was shown that the local charge neutrality gives a so strong constraint that such an exotic state, called the g2SC phase, exists stably;

this is in contrast with the case of the electronic superconductivity in metals [14], where the possible gapless state is unstable against the spatial separation into the Pauli-paramagnetic and superconducting phases because of the absence of a long-range force mediated by gauge fields. The gCFL phase is the three flavor analogue of the g2SC phase. Successive detailed studies have revealed a rich phase structure of superconducting quark matter at zero and nonzero temperatures [15, 16]. It should be also noted that the possible existence of the gCFL phase in a compact star may lead to astronomically interesting consequences because of the existence of the gapless quarks [17]. Thus, examining the robustness of the gapless phases as well as exploring their nature has become one of the central subjects in the study of QCD matter in extreme conditions. In fact, it has been recently indicated [18] that the gluons in the gapless phases acquire an imaginary Meissner mass, which may signal an instability of the system to a yet unknown state.

In this Letter, we investigate how the superconducting orders including the gapless phases are affected by the incorporation of the dynamical chiral condensation. This incorporation should be important when the color superconductivity in a compact star is considered, where a change of the chiral condensate $\langle \bar{q}q \rangle$ is also expected. In fact, the dynamically generated chiral condensate may greatly affect the stability of the gapped superconducting phases, leading to a quite novel phase structure: (i) The interplay between the chiral and diquark condensations makes the quark masses depend on the realized phases [19, 20, 21], and hence some phases in turn become disfavored or favored. (ii) The gapless system might become unstable against the phase separation into the phases with a different chiral condensate $\langle \bar{q}q \rangle$ since the scalar condensate has no gauged charges; recall the fate of the possible gapless state in the electronic superconductors mentioned above [14]. We shall show that the next phase of the CFL phase down in the density is not necessarily the gCFL phase, but strongly depends on the coupling constant in the scalar diquark channel even at zero tem-

*E-mail: abuki@yukawa.kyoto-u.ac.jp

†E-mail: masky@yukawa.kyoto-u.ac.jp

‡E-mail: kunihiro@yukawa.kyoto-u.ac.jp

perature: The gCFL phase is found to appear only in the small coupling regime; this fragileness of the gCFL phase with the dynamical quark condensate will be shown to be understandable in a rather model-independent way. We shall show that the most favorable phases realized in a wide parameter window are the g2SC, 2SC, and unpaired neutral phases.

We start from the following extended three flavor Nambu–Jona-Lasinio (NJL) Lagrangian density with the diquark coupling G_d , and the scalar coupling G_s [13, 21].

$$\begin{aligned} \mathcal{L} = & \bar{q}(i\cancel{\partial} - \mathbf{m}_0 + \boldsymbol{\mu}\gamma_0)q + \frac{G_d}{16} \sum_{\eta=1}^3 [(\bar{q}P_\eta^t \bar{q})({}^t q \bar{P}_\eta q)] \\ & + \frac{G_s}{8N_c} [(\bar{q}\boldsymbol{\lambda}_F q)^2 + (\bar{q}i\gamma_5 \boldsymbol{\lambda}_F q)^2]. \end{aligned} \quad (1)$$

Here, $\boldsymbol{\lambda}_F = \{\sqrt{2/3}\mathbf{1}, \bar{\boldsymbol{\lambda}}_F\}$ are the unit matrix and the Gell-Mann matrices in the flavor space. P_η is defined as in Ref. [12]

$$(P_\eta)_{ij}^{ab} = i\gamma_5 C \epsilon^{\eta ab} \epsilon_{\eta ij} \quad \text{no sum over index } \eta \quad (2)$$

and $\bar{P}_\eta = \gamma_0(P_\eta)^\dagger \gamma_0$. a, b, \dots and i, j, \dots represent the color and flavor indices, respectively. The second term in Eq. (1) simulates the attractive interaction in the color anti-triplet, the flavor anti-triplet and in the $J^P = 0^+$ channel in QCD. $\mathbf{m}_0 = \text{diag}\{m_u, m_d, m_s\}$ is the current-quark mass matrix; the full lattice QCD simulation shows that $m_{u,d}(2 \text{ GeV}) = 3-4 \text{ MeV}$ and $m_s(2 \text{ GeV}) = 80-100 \text{ MeV}$ [22]. We take the chiral SU(2) limit for the u, d sector ($m_u = m_d = 0$) and $m_s = 80 \text{ MeV}$ throughout this paper. These values might slightly underestimate the effect of the current masses.

In order to impose the color and electric neutrality, we introduce the chemical potential matrix $\boldsymbol{\mu}$ in the color-flavor space as

$$\boldsymbol{\mu}_{ij}^{ab} = \mu \delta_{ab} B_{ij} - \mu_e \delta^{ab} Q_{ij} + \mu_3 \delta_{ij} T_3^{ab} + \mu_8 \delta_{ij} T_8^{ab}. \quad (3)$$

$B_{ij} = \delta_{ij}$ and $Q_{ij} = \text{diag}\{2/3, -1/3, -1/3\}$ count baryon number and electric charge of quarks, respectively. $T_3^{ab} = \text{diag}\{1/2, -1/2, 0\}$ and $T_8^{ab} = \{1/3, 1/3, -2/3\}$ are the diagonal generators of the color SU(3). In the numerical analysis, we shall adopt the three-momentum cutoff $\Lambda = 800 \text{ MeV}$ and the scalar coupling constant G_s giving the vacuum constituent quark mass 400 MeV in the chiral limit, for comparison with the results in Refs. [11, 12, 16]; these parameter values give larger condensates than those used in [23] and [13, 21, 24].

We treat the diquark coupling constant G_d as a simple parameter, although the perturbative one-gluon exchange vertex $\mathcal{L}_{\text{int}} = -(g^2/2)\bar{q}\gamma_\mu(\lambda_a/2)q\bar{q}\gamma^\mu(\lambda_a/2)q$, which is valid at extremely high density, tells us that $G_d/G_s = 1/2$ with $N_c = 3$ [21, 25]. Furthermore, we shall use, instead of G_d , the gap energy (Δ_0) in the pure CFL phase at $\mu = 500 \text{ MeV}$ and $T = 0$ in the chiral SU(3) limit, as was done in Refs. [11, 12, 16].

We evaluate the thermodynamic potential in the mean-field approximation;

$$\begin{aligned} \Omega = & \frac{4}{G_d} \sum_{\eta=1}^3 \Delta_\eta^2 + \frac{N_c}{G_s} \sum_{i=1}^3 (M_i - m_i)^2 \\ & - \frac{T}{2} \int \frac{d\mathbf{p}}{(2\pi)^3} \text{Tr} \text{Log} [S^{-1}(i\omega_n, \mathbf{p})] + \Omega_e, \end{aligned} \quad (4)$$

where

$$\begin{aligned} \Delta_\eta &= \frac{G_d}{8} \langle {}^t q P_\eta q \rangle, \\ \mathbf{M} &= \begin{pmatrix} M & 0 & 0 \\ 0 & M & 0 \\ 0 & 0 & M_s \end{pmatrix} \\ &= \mathbf{m}_0 + \frac{G_s}{2} \begin{pmatrix} \langle \bar{u}u \rangle & 0 & 0 \\ 0 & \langle \bar{d}d \rangle & 0 \\ 0 & 0 & \langle \bar{s}s \rangle \end{pmatrix}, \end{aligned} \quad (5)$$

are the gap parameter matrix and the constituent quark mass matrix, respectively, and S denotes the 72×72 Nambu-Gor'kov propagator defined by

$$S^{-1}(i\omega_n, p) = \begin{pmatrix} \not{p} + \boldsymbol{\mu}\gamma_0 - \mathbf{M} & \sum_\eta P_\eta \Delta_\eta \\ \sum_\eta \bar{P}_\eta \Delta_\eta & \not{p} - \boldsymbol{\mu}\gamma_0 + \mathbf{M} \end{pmatrix}, \quad (7)$$

with $\not{p} = i\omega_n \gamma_0 - \mathbf{p} \cdot \boldsymbol{\gamma}$. Finally, Ω_e is the contribution from the massless electrons

$$\begin{aligned} \Omega_e = & -\frac{\mu_e^4}{12\pi^2} \\ & -2T \int \frac{d\mathbf{p}}{(2\pi)^3} \sum_{\xi=\pm} \left[\log(1 + e^{-|\mu_e - \xi p|/T}) \right]. \end{aligned} \quad (8)$$

The functional determinant in Eq. (4) can be evaluated using the method given in the literature [12, 16]. The optimal values of the variational parameters Δ_η , M and M_s must satisfy the stationary condition (the gap equations);

$$\frac{\partial \Omega}{\partial \Delta_\eta} = 0, \quad \frac{\partial \Omega}{\partial M} = 0 \quad \text{and} \quad \frac{\partial \Omega}{\partial M_s} = 0. \quad (9)$$

In order to clarify the effects of the chiral condensation on the diquark pairing, we shall also reexamine the case in which the dynamical chiral condensates are not incorporated [11, 12, 15, 16];

$$\left. \frac{\partial \Omega}{\partial \Delta_\eta} \right|_{\mathbf{m}_0 = \mathbf{M}} = 0. \quad (10)$$

Here the quark mass M_s is regarded as the in-medium strange quark mass and will be varied by hand. Our task is to search the minimum of the effective potential through solving these gap equations under the local electric and color charge neutrality conditions;

$$\frac{\partial \Omega}{\partial \mu_e} = 0, \quad \frac{\partial \Omega}{\partial \mu_3} = 0 \quad \text{and} \quad \frac{\partial \Omega}{\partial \mu_8} = 0. \quad (11)$$

Name of Phase	Gap and mass parameters				Conditions for chemical potentials	Gapless quarks			
	$\Delta_1(ds)$	$\Delta_2(us)$	$\Delta_3(ud)$	M M_s		$(ru-gd-bs)$	$(bd-gs)$	$(bu-rs)$	$(gu-rd)$
CFL (9)	Δ_1	Δ_2	Δ_3	M_s	$[\mu_e = 0]$	all quark modes are fully gapped			
gCFL (7)	Δ_1	Δ_2	Δ_3	M_s	$\delta\mu_{bd-gs(bu-rs)} + \frac{M_s^2}{4\mu} \gtrsim \Delta_{1(2)}$	bd	bu		
uSC (6)		Δ_2	Δ_3	M_s	$[\mu_e = 0]$	$gd-bs$ (1)	(bd, gs)		
guSC (5)		Δ_2	Δ_3	M_s	$\delta\mu_{bu-rs} + \frac{M_s^2}{4\mu} \gtrsim \Delta_2$	$gd-bs$ (1)	(bd, gs)	bu	
2SC (4)			Δ_3	M_s	$[\mu_3 = 0]$	bs	(bd, gs)	(bu, rs)	
g2SC (2)			Δ_3	M_s	$[\mu_3 = 0], \delta\mu_{gd-ru} = \delta\mu_{rd-gu} > \Delta_3$	gd, bs	(bd, gs)	(bu, rs)	rd
dSC (6)	Δ_1		Δ_3	M_s		$ru-bs$ (1)		(bu, rs)	
gdSC (5)	Δ_1		Δ_3	M_s	$\delta\mu_{bd-gs} + \frac{M_s^2}{4\mu} \gtrsim \Delta_1$	$ru-bs$ (1)	bd	(bu, rs)	
2SCus (4)		Δ_2		M_s		gd	(bd, gs)	(bu, rs)	
UQM (0)				M_s	$[\mu_3 = \mu_8 = 0]$	all quarks are ungapped.			
χ SB (0)				M M_s	$[\mu_3 = \mu_8 = 0]$	all quarks are massive.			

TABLE I: The nonzero gap parameters, some conditions between gaps and chemical potentials, and the gapless quarks in each phase. We abbreviate the unpaired neutral quark matter with nonzero $\langle \bar{s}s \rangle$ to “UQM”, and the chiral-symmetry broken phase as “ χ SB”, respectively. (g) means the gapless version of the pairing state. The number in the parenthesis in the first column represents the number of gapped quasi-quark modes. “ $gd-bs$ (1)” means that one of the linear combination of gd and bs quarks remains gapless. $\delta\mu_{gd-bs}$ denotes the chemical potential difference $\equiv (\mu_{gd} - \mu_{bs})/2$, and so forth. The equations for chemical potentials which are necessarily satisfied in the given phase are written in a bracket in the third column.

Before going into a numerical computation, one must specify the phase characterized by the various patterns of the mean fields and the chemical potentials (μ_e, μ_3, μ_8) ; comparing the value of Ω obtained for each phase, one can determine which phase is realized for given μ and Δ_0 . In the present analysis, we consider the states listed in TABLE I as possible phases to be realized. These phases are described in the following sub-model spaces defined by the parameter sets in the parenthesis, respectively; within which the gap equation for each phase is solved.

Set. 1 (μ_e, M, M_s) : This parameter space can model the χ SB phase and the neutral unpaired quark matter (UQM). The dynamical condensates in all flavor sectors ($\langle \bar{u}u \rangle, \langle \bar{d}d \rangle, \langle \bar{s}s \rangle$) are accompanied in the χ SB phase, while in the UQM phase, only $\langle \bar{s}s \rangle$ is non-vanishing.

Set. 2 $(\Delta_3, \mu_e, \mu_8, M_s)$: In this parameter space, the (g)2SC and UQM phases are described.

Set. 3 $(\Delta_2, \mu_e, \mu_3, \mu_8, M_s)$: The 2SCus and UQM phases are described in this parameter space.

Set. 4 $(\Delta_2, \Delta_3, \mu_e, \mu_3, \mu_8, M_s)$: The (g)uSC, (g)2SC and UQM phases are described in this space.

Set. 5 $(\Delta_1, \Delta_3, \mu_e, \mu_3, \mu_8, M_s)$: The (g)dSC, (g)2SC and UQM phases are described in this space [26].

Set. 6 $(\Delta_1, \Delta_2, \Delta_3, \mu_e, \mu_3, \mu_8, M_s)$: The (g)CFL, (g)uSC and UQM phases are described in this space.

We numerically confirmed that other phases such as 2SCds or sSC phases, which are described with the parameter set $(\Delta_1, \mu_e, \mu_3, \mu_8)$ or $(\Delta_1, \Delta_2, \mu_e, \mu_3, \mu_8)$, respectively, never get realized as the ground state at $T = 0$. In this Letter, we restrict ourselves to the zero temperature case, leaving an analysis on the $T \neq 0$ case for a future publication.

We first present the phase diagram *without* the dynamical chiral condensates with M_s being varied by hand for a fixed quark chemical potential $\mu = 500$ MeV; the ground

state is searched with the aid of the gap equation Eq. (10) which gives a candidate of the ground state. FIG. 1(a) shows an entire phase diagram in the $(M_s^2/\mu, \Delta_0)$ plane; we notice that this phase diagram is consistent with the one given in [16], in which the phase structure only for several values of Δ_0 is given. One may notice the following points:

(1) The gCFL phase always exists as the next phase of the CFL phase down in density, irrespective of the value of the diquark coupling Δ_0 . In addition, the parameter region of M_s^2/μ for accommodating the gCFL phase grows as the diquark coupling constant increases.

(2) The stronger the coupling Δ_0 , the richer the phase structure: The CFL phase turns into the UQM phase through successive transitions; gCFL \rightarrow guSC \rightarrow 2SC \rightarrow g2SC. Accordingly, the number of frozen degrees of freedom (gapped quarks) decreases as $9 \rightarrow 7 \rightarrow 5 \rightarrow 4 \rightarrow 2 \rightarrow 0$ towards lower density.

Now let us examine how the above features are changed once the strange quark mass is determined dynamically through Eq. (9). The resulting phase diagram in the (μ, Δ_0) plane is shown in FIG. 1(b); M_s is now determined dynamically and thus becomes a function of μ and Δ_0 . The following should be notable from the figure:

(1) Although the CFL phase is present still in all the diquark coupling region, the chemical potential window for realizing the gCFL phase shrinks with the increasing coupling constant, and eventually closes at $\Delta_0 \sim 50$ MeV. This is highly in contrast with the case described above.

(2) As the coupling is increased, the following phases appear successively as the next phase of the CFL phase down in density; the gCFL phase, the UQM phase, the g2SC phase, and finally the 2SC phase.

We can clearly divide the entire phase diagram into four distinct regions according to which phase comes in as the next phase down from the CFL phase. (i) The *weak*

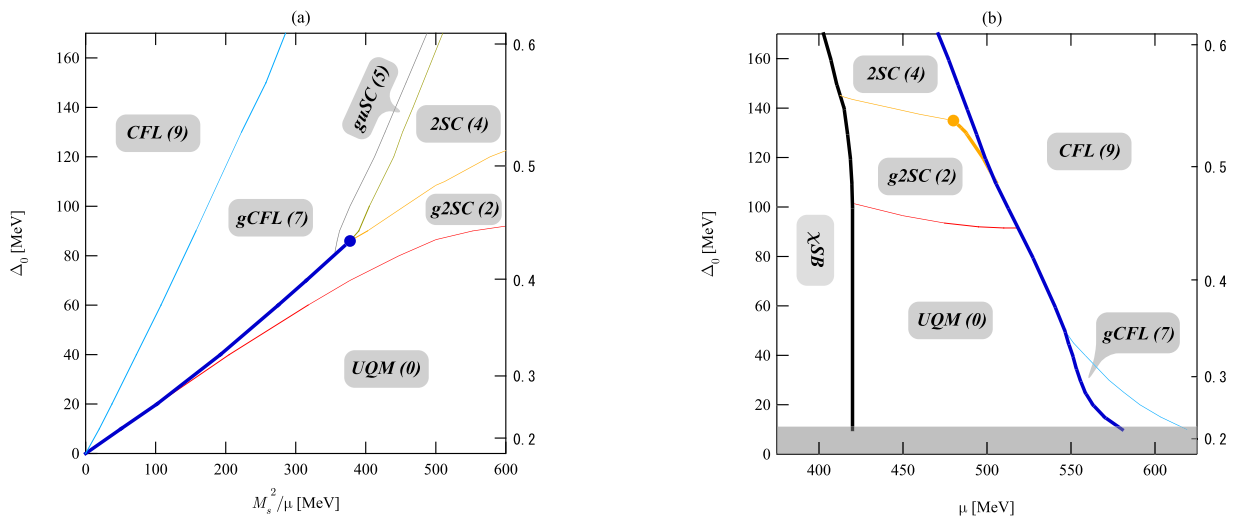


FIG. 1: (a) Phase diagram in $(\Delta_0, M_s^2/\mu)$ plane: The gap equations Eq. (10) under the neutrality constraints are solved with varying $M_s = m_s$ by hand, while the quark chemical potential is fixed at $\mu = 500$ MeV as in Refs. [11, 12, 15, 16]. The scale of the vertical axis on the right-hand side represents the value of $\eta = G_d/G_s$ for the corresponding diquark coupling Δ_0 . The number in a parenthesis attached to each phase name in the figure denotes the number of gapped quasi-quarks. (b) Phase diagram in (Δ_0, μ) plane: Continuous (first order) transition lines are represented by thin (bold) lines. Although we did not determine the phase boundaries in the dark-shaded area where a rather better precision is required for the comparison of the potentials, we confirmed that any new phase structure does not appear in this region.

coupling regime ($\Delta_0 \lesssim 50$ MeV); the gCFL phase exists between the UQM and CFL phases. (ii) The *moderate coupling regime* ($50 \text{ MeV} \lesssim \Delta_0 \lesssim 90$ MeV); the gCFL phase ceases to be the secondly densest phase, and is taken over by the UQM phase, which is nearly two-flavor quark matter with large $\langle \bar{s}s \rangle$ condensate. We stress that the superconductivity itself is destroyed before the gCFL phase sets in when the density is decreased. (iii) The *strong coupling regime* ($90 \text{ MeV} \lesssim \Delta_0 \lesssim 140$ MeV); a gapless superconducting phase reappear but only with the two flavors being involved, which is called the g2SC phase. Also a large chiral condensate $\langle \bar{s}s \rangle$ is accompanied in this phase. (iv) The *extremely strong coupling regime* ($140 \text{ MeV} \lesssim \Delta_0$); any gapless superconductivity vanishes and the fully-gapped 2SC phase is realized. It is worth mentioning that the $g2SC \rightarrow 2SC$ transition with the increasing diquark coupling near the CFL phase seen in Fig. 1(b) is not of a second order but of a first order with a small jump in the strange quark mass and density. The first order phase transition ends at the point denoted by a large dot in FIG. 1(b). For smaller chemical potential than that at this point, the $2SC \rightarrow g2SC$ transition is continuous and essentially the same as that found in the original paper [13], because the on-shell strange quarks are not present in this region due to a large dynamical mass of the strange quark.

So far the global structure of the phase diagram. Next let us discuss in detail how the gCFL phase disappears for the stronger diquark coupling, examining closely two typical coupling cases; $\Delta_0 = 25$ MeV (*weak coupling*), $\Delta_0 = 60$ MeV (*moderate coupling*). We shall also show the μ dependence of gaps in the phases which are actually

not realized as the ground state, for completeness.

FIG. 2(a) shows the gap parameters as functions of μ for several phases. At high chemical potentials $\mu \gtrsim 580$ MeV, the ground state is in the CFL phase. As the density is decreased, the stress energy $M_s^2(\mu)/\mu$ increases in the symmetric CFL pairing; notice that as the density is decreased, the in-medium strange quark mass $M_s(\mu)$ increases, which causes a further increase of the stress $M_s^2(\mu)/\mu$. Accordingly, the phase suffers from a slight distortion in the gaps ($\Delta_1 = \Delta_2 \lesssim \Delta_3$); nevertheless the CFL phase persists down to the critical chemical potential $\mu = \mu_* \cong 581.1$ MeV, at which the effective chemical potential difference in $(bd-gs)$ sector, $\delta\mu_{\text{eff}}(bd-gs) \equiv \delta\mu_{bd-gs} + \frac{M_s^2}{4\mu}$, reaches almost the magnitude of the gap $\Delta_1 = \Delta_2$. This transition is essentially the \bar{Q} -insulator-to-metal transition discussed in [11, 12], with \bar{Q} being the unbroken U(1) charge in the CFL phase [3, 4]. We notice that the onset condition of this metal-insulator transition, $M_s^2(\mu_*)/2\mu_* \cong \Delta_1(\mu_*)$ [11], works well even when the strange quark mass is treated as a dynamical variable. As the density is decreased further, the UQM phase with massive strange quarks finally takes over the gCFL phase at $\mu \cong 558$ MeV, which is denoted by the dashed line in FIG. 2. This unlocking transition $gCFL \rightarrow UQM$ is a first order as was found in Refs. [11, 12, 16], although the transition point is somewhat shifted to a lower $M_s(\mu)$ (higher μ) than is obtained in these papers.

FIG. 2(b) shows the state-dependent strange quark mass as a function of μ in the (g)CFL and the UQM phases. One should notice that the generation of the dynamical strange quark mass is suppressed in the (g)CFL

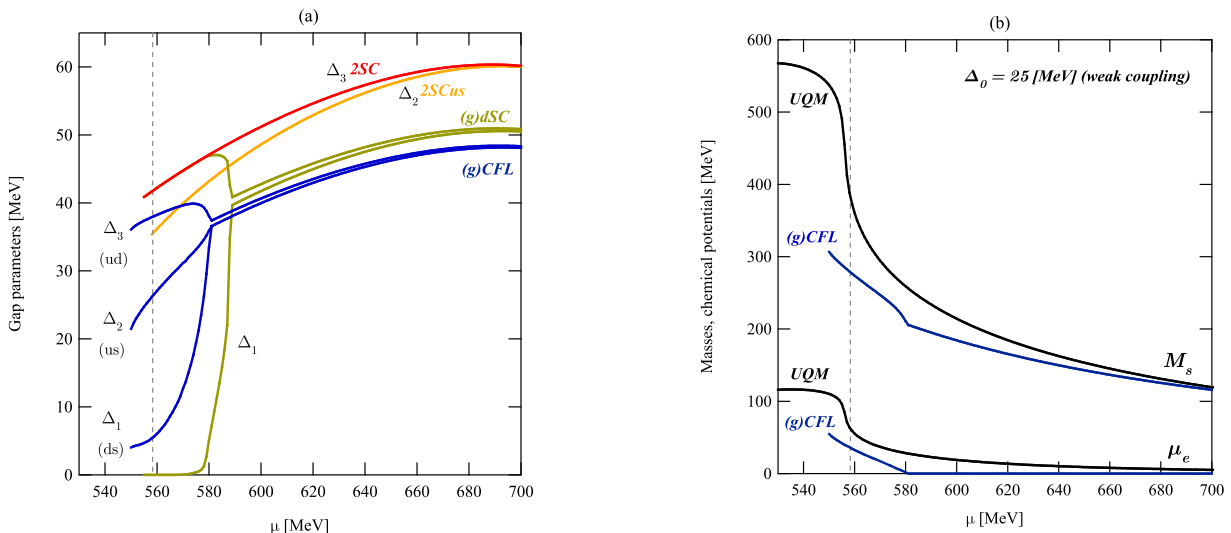


FIG. 2: (a) The gap parameters for each state at a weak coupling $\Delta_0 = 25$ MeV. We remark that the states other than the (g)CFL and UQM phases are realized only as metastable states for all the region of μ ; nevertheless the 2SC, 2SCus and (g)dSC phases give the global minimum in the corresponding sub-model spaces, namely, Set. 2, Set. 3, and Set. 5, respectively. The vertical dashed line represents the point $\mu \cong 558$ MeV where the UQM phase takes over the gCFL phase, below which the UQM phase with massive strange quarks accordingly becomes the ground state of the system. The CFL phase turns into the gapless CFL phase at the critical chemical potential $\mu = \mu_* = 581.1$ MeV. (b) The state-dependent strange quark masses and the electron chemical potentials for the (g)CFL and UQM phases at the same coupling as in (a).

phase in comparison with that in the UQM phase. This is because the (g)CFL pairing requires a Fermi-momentum matching among all the species as much as possible, which is achieved by suppressing the dynamical generation of the strange quark mass; it is also to be noticed that a better Fermi-momentum matching also lowers the energy cost for imposing charge neutrality. On the other hand, the UQM phase does not need such a Fermi-momentum matching, and thus can gain the condensation energy in the chiral $\langle \bar{s}s \rangle$ sector. In other words, the first-order unlocking gCFL \rightarrow UQM phase transition is brought about by the competition between the following two factors; (i) reducing the neutrality costs by matching the Fermi momenta of three species in the gCFL phase, and (ii) increasing the condensation energy gain in the chiral $\langle \bar{s}s \rangle$ sector in the UQM phase. The former effect (i) is underestimated in the previous work [11, 12, 16] because the strange quark mass is treated as a simple parameter, i.e., $M_s(\text{UQM}) = M_s(\text{CFL})$. The latter effect (ii) is taken into account for the first time in the present work. As a consequence, the transition density (strange quark mass) is somewhat larger (smaller) in comparison with the results in [11, 12, 16]; in fact the transition takes place at $M_s^2/\mu \sim 4\Delta_1(\mu_*)$ in the present work, while $M_s^2/\mu \sim 5\Delta_1(\mu_*)$ in Refs. [11, 12, 16], with $\Delta_1(\mu_*)$ being the gap in the $(bd\text{-}gs)$ sector at the onset point of the gCFL phase. We emphasize that this tendency of destabilizing the (g)CFL phase by the dynamical generation of chiral condensate should hold generically, not depending on a model used.

How do the above features change when the diquark

coupling is raised? One might naively expect that the window in μ for the gCFL realization becomes wide, thinking that the gCFL phase should become more robust in the stronger coupling regime. It is, however, not the case; in fact, we have no longer a window for the gCFL phase in the moderate coupling, for instance, at $\Delta_0 = 60$ MeV. (See FIG. 1(b).) This disappearance of the gCFL phase in the stronger coupling can be nicely understood with the aid of the thermodynamic potential. In FIG. 3, we show the thermodynamic potentials for the UQM phase and the CFL phases with $\Delta_0 = 25, 35, 50,$ and 70 MeV. We first notice that $\mu = M_s^2(\mu_*)/2\Delta_1(\mu_*)$ denoted by large dots on the horizontal axis gives a quite good guide for the critical chemical potential μ_* for the CFL-gCFL transition. Accordingly, the transition point shifts to a lower μ as the diquark coupling is increased and eventually moves to the left of the UQM line which rapidly falls for $\mu \lesssim 550$ MeV because of the quite large chiral condensate realized in the UQM phase as is clearly seen in FIG. 2(b). In particular, for $\Delta_0 = 70$ MeV, the CFL phase becomes metastable against the UQM phase before the gCFL phase sets in. In other words, the UQM phase takes over the CFL phase before the gapless dispersions of bd and bu quarks get to be realized. In short, although the CFL phase becomes more stable with the larger diquark coupling, making the gCFL-CFL transition point μ_* lower, the UQM phase overwhelms all the paired phases because of the large $\langle \bar{s}s \rangle$ -condensation energy. We also remark that at the end points of the (g)CFL lines in FIG. 3, the (g)CFL states cease to exist even as a metastable state, nor as a

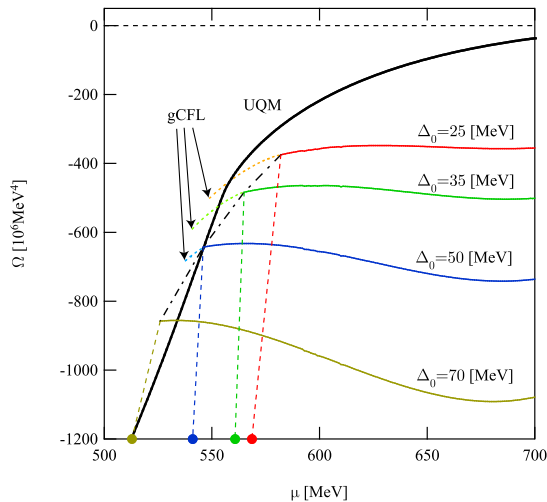


FIG. 3: The thermodynamic potentials Ω for the UQM phase and the CFL phases with various couplings as functions of μ . We have chosen the zero of the potential such that the unpaired neutral quark matter with bare ($M_s = 80$ MeV) strange quarks has $\Omega = 0$. The CFL phases turn into the gapless phases at the points where the bold lines change into the dashed lines. These gCFL-CFL transition points are linked by the dash-dotted line. In the horizontal axis, we also put large dots, which denote the values $M_s^2(\mu_*)/2\Delta_1(\mu_*)$ for corresponding Δ_0 .

local maximum like the unstable Sarma state [14].

Finally let us see the reason why the (g)2SC phase comes as the next phase down in density as the diquark coupling is increased further. As the coupling is increased, the UQM phase is expected to experience successive second order phase transitions firstly to the g2SC phase and then to the 2SC phase if the strange quarks are not present in the system [13]. Our full calculation shows that the on-shell strange quarks are absent in the system at $\mu \lesssim 450$ MeV because of a large M_s ; thus the series of transitions UQM \rightarrow g2SC \rightarrow 2SC becomes essentially the same as in [13]. At relatively higher chemical potential, however, the small amount of the strange quarks are present, which brings about a non-trivial tricritical point on the g2SC \rightarrow 2SC transition line in the phase diagram (see the large dot in FIG. 1(b)). At higher μ than this point, the g2SC \rightarrow 2SC transition is a first order with jumps in physical quantities as mentioned before. We notice that this first order transition is also caused by the competition between the chiral $\langle \bar{s}s \rangle$ condensation in the g2SC phase and the pairing energy gain in the fully gapped 2SC order. In fact, the transition is from a 2SC phase (2SC+s) with a small strange quark density to a nearly two-flavor g2SC phase with larger vacuum $\langle \bar{s}s \rangle$ condensate along the first order line. The 2SC phase tends to lower the density mismatch between n_u and n_d , and thus needs more strange quarks as well as electrons for the electric neutrality than in the g2SC phase. As a

result, the 2SC+s phase tends to reduce the dynamical strange quark mass. In contrast, the g2SC phase has extra d quarks accumulated in the momentum shell, thus requires less strange quarks. For this reason, the g2SC phase can have a larger dynamical chiral condensate $\langle \bar{s}s \rangle$.

In this Letter, we have made an analysis on the interplay between the chiral and diquark condensations in the three-flavor neutral quark matter using an extended NJL model. We have shown that which phase appears next to the CFL phase strongly depends on the strength of the diquark coupling; as the diquark coupling is increased, the gCFL, the UQM, the g2SC and finally the 2SC phase appear as the next phase down in density. The disappearance of the gCFL phase in the strong coupling regime and the emergence of a non-trivial tricritical point on the 2SC \rightarrow g2SC transition line are qualitatively understandable in terms of the competition among the chiral-condensation energy, the gain through the pairing and the energy cost due to neutrality constraints. Although the present calculation is performed with a specific value of the cutoff $\Lambda = 800$ MeV, we have confirmed that our central result, namely, the shrinkage of the gCFL window with the increasing diquark coupling, is unaffected with the change of Λ in the range $600 \sim 1000$ MeV. In a longer paper, we shall present a more detailed analysis on the nature of phase transitions obtained here, giving some physical quantities including strange and isospin densities in each phase.

In the present work, we have restricted ourselves to the case with vanishing temperature. It would be interesting to study the competition between the chiral and diquark condensations at finite temperature, and to examine the robustness or fragileness of the phases obtained here. The extension of this work to the nonzero temperature is straightforward and will be discussed elsewhere. Finally, we have not considered here the possibility of the quantum inhomogeneous state [27, 28] and the possible meson condensation in the CFL phase [29] from the beginning. Also we did not take care of a potential instability due to the imaginary Meissner mass in the gapless phases [18]. A detailed analysis including all these possibilities is certainly a challenge but needed for our deeper understanding of the QCD phase diagram.

The authors are grateful to M. Alford for his interest in this work and valuable comments which led to FIG. 3. One of the authors, H. A. thanks M. Asakawa for encouragement. H. A. is supported by the Fellowship program, Grant-in-Aid for the 21COE, “Center for Diversity and Universality in Physics” at Kyoto University. M. K. is supported by Japan Society for the Promotion of Science for Young Scientists. T. K. is supported by Grant-in-Aide for Scientific Research by Monbu-Kagaku-sho (No. 14540263). This work is supported in part by a Grant-in-Aid for the 21st Century COE “Center for Diversity and Universality in Physics”.

-
- [1] D. Bailin and A. Love, *Phys. Rept.* **107**, 325 (1984).
- [2] M. Iwasaki and T. Iwado, *Phys. Lett. B* **350**, 163 (1995).
- [3] For reviews, see K. Rajagopal and F. Wilczek, arXiv:hep-ph/0011333; M.G. Alford, *Ann. Rev. Nucl. Part. Sci.* **51**, 131 (2001); G. Nardulli, *Riv. Nuovo Cim.* **25N3**, 1 (2002); S. Reddy, *Acta Phys. Polon. B* **33**, 4101 (2002); T. Schäfer, arXiv:hep-ph/0304281; M. Alford, arXiv:nucl-th/0312007.
- [4] M.G. Alford, K. Rajagopal and F. Wilczek, *Nucl. Phys.* **B537**, 443 (1999).
- [5] K. Iida and G. Baym, *Phys. Rev. D* **63**, 074018 (2001); Erratum-ibid. *D* **66**, 059903 (2002).
- [6] K. Rajagopal and F. Wilczek, *Phys. Rev. Lett.* **86**, 3492 (2001).
- [7] M. Alford and K. Rajagopal, *JHEP* **0206**, 031 (2002).
- [8] M. Alford, J. Berges and K. Rajagopal, *Nucl. Phys.* **B558**, 219 (1999).
- [9] T. Schäfer and F. Wilczek, *Phys. Rev. D* **60**, 074014 (1999).
- [10] H. Abuki, *Prog. Theor. Phys.* **110**, 937 (2003).
- [11] M. Alford, C. Kouvaris and K. Rajagopal, *Phys. Rev. Lett.* **92**, 222001 (2004).
- [12] M. Alford, C. Kouvaris and K. Rajagopal, arXiv:hep-ph/0406137.
- [13] I. Shovkovy and M. Huang, *Phys. Lett. B* **564**, 205 (2003); M. Huang and I. Shovkovy, *Nucl. Phys.* **A729**, 835, (2003).
- [14] G. Sarma, *Phys. Chem. Solid* **24**, 1029 (1963).
- [15] S.B. Ruster, I. Shovkovy and D. Rischke, *Nucl. Phys.* **A743**, 127 (2004).
- [16] K. Fukushima, C. Kouvaris and K. Rajagopal, arXiv:hep-ph/0408322.
- [17] M. Alford, P. Jotwani, C. Kouvaris, J. Kundu and K. Rajagopal, arXiv:astro-ph/0411560.
- [18] M. Huang and I. Shovkovy, *Phys. Rev. D* **70**, 094030 (2004); *Phys. Rev. D* **70**, 051501 (2004); R. Casalbuoni, R. Gatto, M. Mannarelli, G. Nardulli and M. Ruggieri, *Phys. Lett. B* **605**, 362 (2005); I. Giannakis and H.C. Ren, arXiv:hep-ph/0412015; for a general argument on the emergence of the imaginary Meissner mass in a gapless phase, see, M. Alford and Q. Wang, arXiv:hep-ph/0501078.
- [19] H. Abuki, Master thesis submitted to Kyoto University (2000).
- [20] M. Kitazawa, T. Koide, T. Kunihiro and Y. Nemoto, *Prog. Theor. Phys.* **108**, 929 (2002).
- [21] A.W. Steiner, S. Reddy and M. Prakash, *Phys. Rev. D* **66**, 094007 (2002).
- [22] CP-PACS, *Phys. Rev. D* **65**, 054505 (2002).
- [23] T. Hatsuda and T. Kunihiro, *Phys. Rept.* **247**, 221 (1994).
- [24] M. Buballa, arXiv:hep-ph/0402234.
- [25] M. Buballa and M. Oertel, *Nucl. Phys.* **A703**, 770 (2002).
- [26] K. Iida, T. Matsuura, M. Tachibana and T. Hatsuda, *Phys. Rev. Lett.* **93**, 132001 (2004); see K. Iida, T. Matsuura, M. Tachibana and T. Hatsuda, *Phys. Rev. D* **71**, 054003 (2005) and [16] for recent developments.
- [27] M.G. Alford, J.A. Bowers and K. Rajagopal, *Phys. Rev. D* **63**, 074016 (2001); For a review, see R. Casalbuoni and G. Nardulli, *Rev. Mod. Phys.* **76**, 263 (2004), and references therein.
- [28] S. Reddy and G. Rupak, arXiv:nucl-th/0405054.
- [29] P.F. Bedaque and T. Schäfer, *Nucl. Phys.* **A697**, 802 (2002); D.B. Kaplan and S. Reddy, *Phys. Rev. D* **65**, 054042 (2002).